Materials Research Letters

ISSN: 2166-3831 (Online) Journal homepage: www.tandfonline.com/journals/tmrl20

An Ideal Ultrafine-Grained Structure for High Strength and High Ductility

C. X. Huang, W. P. Hu, Q. Y. Wang, C. Wang, G. Yang & Y. T. Zhu

To cite this article: C. X. Huang, W. P. Hu, Q. Y. Wang, C. Wang, G. Yang & Y. T. Zhu (2015) An Ideal Ultrafine-Grained Structure for High Strength and High Ductility, Materials Research Letters, 3:2, 88-94, DOI: 10.1080/21663831.2014.968680

To link to this article: https://doi.org/10.1080/21663831.2014.968680

© 2014 The Author(s). Published by Taylor & Francis.

View supplementary material

Published online: 09 Oct 2014.

Submit your article to this journal

Article views: 6583

View related articles

View Crossmark data

Citing articles: 28 View citing articles

Full Terms & Conditions of access and use can be found at
https://www.tandfonline.com/action/journalInformation?journalCode=tmrl20

MATERIALS RESEARCH LETTERS

Mater. Res. Lett., 2015
Vol. 3, No. 2, 88–94, http://dx.doi.org/10.1080/21663831.2014.968680

Taylor & Francis
Taylor & Francis Group

www.tandfonline.com/toc/tmrl20/current

An Ideal Ultrafine-Grained Structure for High Strength and High Ductility

C. X. Huang[a*], W. P. Hu[b], Q. Y. Wang[c*], C. Wang[d], G. Yang[d] and Y. T. Zhu[e,f]

[a]School of Aeronautics and Astronautics, Sichuan University, Chengdu 610065, People's Republic of China; [b]Institute of Physical Metallurgy and Metal Physics, RWTH Aachen University, Aachen 52056, Germany; [c]Institute for Mechanics of Advanced Materials and Structures, Chengdu University, Chengdu 610106, People's Republic of China; [d]Central Iron and Steel Research Institute, Beijing 100081, People's Republic of China; [e]Department of Materials Science and Engineering, North Carolina State University, Raleigh, NC 27695, USA; [f]School of Materials Science and Engineering, Nanjing University of Science and Technology, Nanjing 210094, People's Republic of China

(*Received 7 July 2014; final form 18 September 2014*)

Supplementary Material Available Online

An ideal ultrafine-grained (UFG) microstructure for high strength and high ductility should have short dislocation-slip path to impede dislocation slip and very low dislocation density to ensure more room for dislocation accumulation. Such a microstructure is hard to produce, especially for UFG metals produced by severe plastic deformation techniques. Here, we report an ideal UFG structure produced by reverse transformation of deformation-induced martensite in 304 L austenitic stainless steel. It produced small grains and a high density of nanotwins for both high strength and high ductility. This approach is applicable to face-centered cubic metals with low stacking fault energy.

Keywords: Ultrafine Grains, Dislocations, Twins, Stacking Faults, Strength and Ductility

What is an ideal ultrafine-grained (UFG) structure for high strength and high ductility? First, to produce high strength in a pure metal or alloy, the path for free slip of dislocations needs to be short to make it hard for dislocation to slip. In other words, high spatial density of barriers to block dislocation slip is needed. Second, to produce high tensile ductility, effective accumulation of crystalline defects such as dislocations, stacking faults (SFs) and/or twin boundaries (TBs) is needed to produce a high strain-hardening rate to deter necking under tensile strain.[1–3] This requires microstructures that can effectively accumulate crystalline defects such as dislocations and have initial low dislocation density to leave enough room for dislocation accumulation.

It is a challenge to produce UFG microstructures with the ideal characteristics described above, especially in large work pieces. UFG metals and alloys are usually produced by a top-down approach named severe plastic deformation (SPD) because it can produce bulk UFG work pieces that are large enough for real-world structural applications at reasonably low cost.[4] SPD techniques refine grains by plastically deforming a metal to extremely large plastic strain, which results in dislocation rearrangement and grain subdivision.[5–7] Consequently, high density of dislocations often exists in the as-processed UFG metals,[8,9] which leaves little room for further dislocation accumulation. This leads to low strain hardening and low ductility, which has been reported in UFG materials produced by the SPD methods such as equal channel angular pressing (ECAP),[10] accumulative roll bonding [11–13] and high pressing torsion.[14] Annealing UFG metals to lower dislocation density can recover some of the ductility, but often at the cost of significant reduction in strength.[15,16] In addition, some dislocation structures produced by SPD could be relatively stable and hard to be fully annealed out without significant grain growth, which dramatically decreases the strength.[17]

Here, we report an ideal UFG microstructure in 304 L austenitic stainless steel (304 L SS) that was

*Corresponding author. Email: chxhuang@scu.edu.cn, wangqy@scu.edu.cn

© 2014 The Author(s). Published by Taylor & Francis.
This is an Open Access article distributed under the terms of the Creative Commons Attribution License (http://creativecommons.org/licenses/by/3.0), which permits unrestricted use, distribution, and reproduction in any medium, provided the original work is properly cited. The moral rights of the named author(s) have been asserted.

produced by reverse transformation of deformation-induced martensite. This UFG microstructure is composed of fine grains and high density of twins to ensure high strength, while its low dislocation density leaves more room for strain hardening. Furthermore, the low stacking fault energy (SFE) of 304 L SS leads to simultaneous accumulation of both dislocations and SFs, making it more effective in strain hardening. As a result, a combination of high yield strength (810 MPa) and high uniform elongation (30%) is obtained in tensile tests.

The 304 L SS has a composition (wt%) of 0.007 C, 18.46 Cr, 11.82 Ni, 1.61 Si, 0.008 S, 0.018 P, 0.29 Mn and the balance Fe. The UFG microstructure was produced by means of phase-reversion annealing of heavily cold-deformed austenite.[18,19] Specifically, the coarse-grained (CG) samples were first processed by ECAP at room temperature (RT) for six passes, which produced a high volume fraction ($\sim$70%) of deformation-induced martensite with a mean grain size of $\sim$90 nm.[20] This was followed by annealing at 625°C for 60 min, which reversely transformed all martensite back to austenite with ultrafine grain sizes and high density of nanotwins. Figure 1(a) shows the typical transmission electron microscopy (TEM) image of the phase-reverted microstructure with a mean grain size of 660 nm. It reveals equiaxed grains with sharp grain boundaries (GBs), annealing nanotwins, and very low dislocation density. Approximately 75% of grains were observed containing annealing nanotwins in the TEM micrograph. The actual fraction of grains that contain annealing twins should be higher since some twins without appropriate orientation may be not observed under TEM.[21] Figure 1(b) is an electron back scattered diffraction (EBSD) image, which shows a high fraction of the Σ3 TBs, as marked with red lines. The average thickness of the twins is $\sim$110 nm, as shown in Figure 1(c). The GB misorientation distribution is shown in Figure 1(d). Ignoring the boundaries with misorientation less than 2°, the high-angle GBs ($>$15°) comprise 92% of the total GBs. The highest peak at $\sim$60° results from Σ3 TBs, which is 23.1% of the total boundaries.

By uniaxial tensile testing at RT, the yield strength and ultimate tensile strength of the UFG samples were measured to be 810 and 970 MPa, respectively. The high yield strength can be attributed to fine grain sizes, according to the Hall–Petch relationship. In addition,

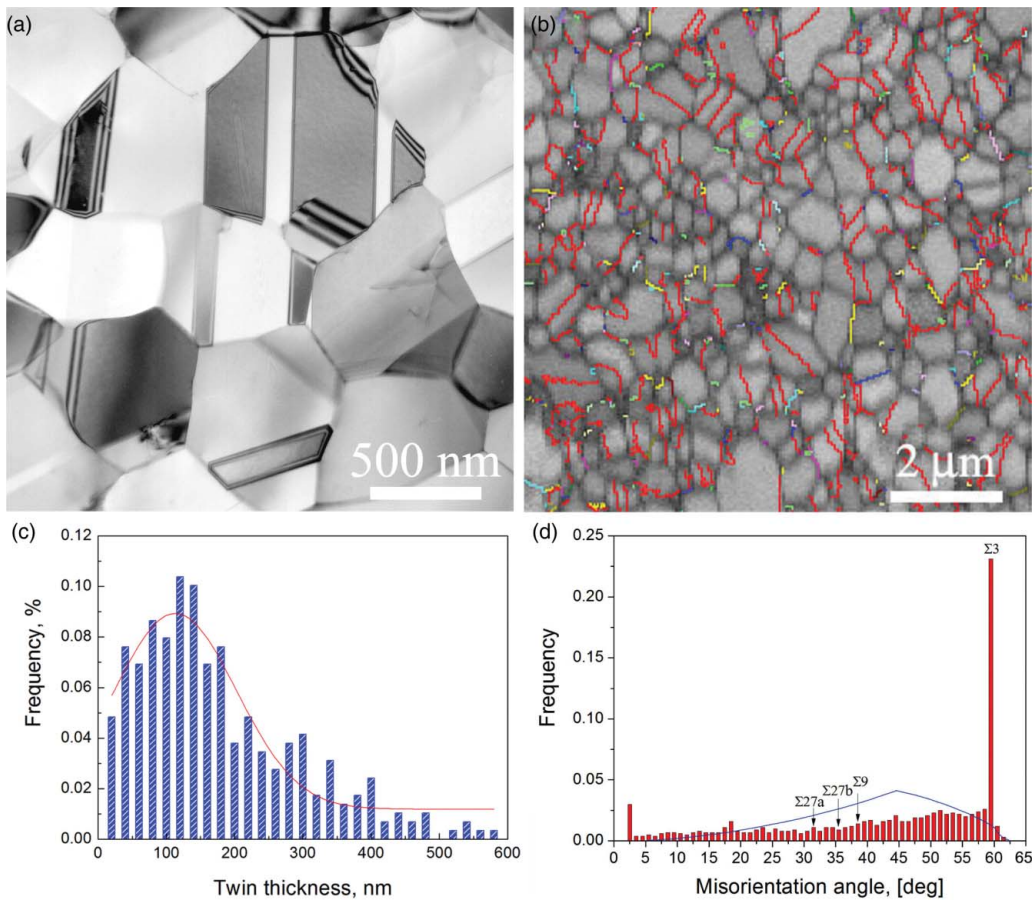

Figure 1. (a) Typical TEM micrograph showing the UFG microstructure produced by phase reversion transformation, (b) EBSD image. The black lines denote random GBs and the colored lines represent coincident-site lattice boundaries, of which the Σ3 TBs are represented by red lines, (c) distribution of twin thickness, (d) distribution of GB misorientation angles.

the high density of nanotwins should also have contributed to the observed high yield strength, because TBs play a similar role to that of GBs.[22,23] A high uniform elongation of 30% was obtained, which is much higher than that of most UFG materials.[8–14] Figure 2(a) shows the representative true stress–strain curves of the current ideal UFG 304 L sample and its CG counterpart. The samples used for tensile tests are in dog-bone shape with gauge dimensions of $1 \times 2 \times 8\ mm^3$ (see Figure S1 in the Supplementary material). A yield drop in stress is observed in the UFG sample, suggesting a strong pinning of mobile dislocations, which underpins the high yield stress. After yielding, the Lüders deformation is activated for a few percent of strain with low strain-hardening rate (see Figure S1).With further straining, the UFG sample undergoes high strain hardening, which produces a large uniform plastic deformation. X-ray diffraction analysis at tensile strains of 10.9%, 19.2% and 29.3% revealed no strain-induced martensite (see Figure S2), indicating that no martensitic transformation occurred during tensile deformation. It has been reported that decreasing austenite grain size can enhance the austenite stability to impede strain-induced martensite transformation.[24,25] In addition, the relatively high nickel and very low carbon contents in this 304 L steel also improved the austenite stability. Therefore, the high strain-hardening rate of the current UFG sample was caused by the accumulation of dislocations and/or other crystalline defects.

Figure 2(b) compares the yield strength and uniform elongation of the current sample with those reported in the literature for 304 L SSs with Ni concentration in the range of 10–12%.[26–30] As shown, for most reported data points, the yield strength usually decreases with increasing uniform elongation. However, the strengths-uniform elongations of the current UFG samples are clearly superior to those reported in literature. The only other data point (the pink triangle [30]) that is comparable to the current one is from a sample that had strain-induced martensite transformation during tensile deformation. It has been reported that the strain-induced martensite causes undesired hydrogen embrittlement [31–33] and decreases corrosion resistance of austenitic SSs.[34–36] These problems are avoided in the current ideal UFG sample, which has more stable austenite due to ultrafine grain sizes.

In order to identify the deformation mechanism, the UFG samples after tensile testing were characterized by TEM and high-resolution TEM (HRTEM). Figure 3(a) shows the typical microstructure at low magnification after ~28% tensile strain. It reveals very high dislocation density, in sharp contrast with the initial microstructure before testing (Figure 1(a)). Figure 3(b) further shows the defect structure in the interior of a single grain at higher magnification by tilting the incident beam to parallel to the [011] zone axis. It reveals a high density

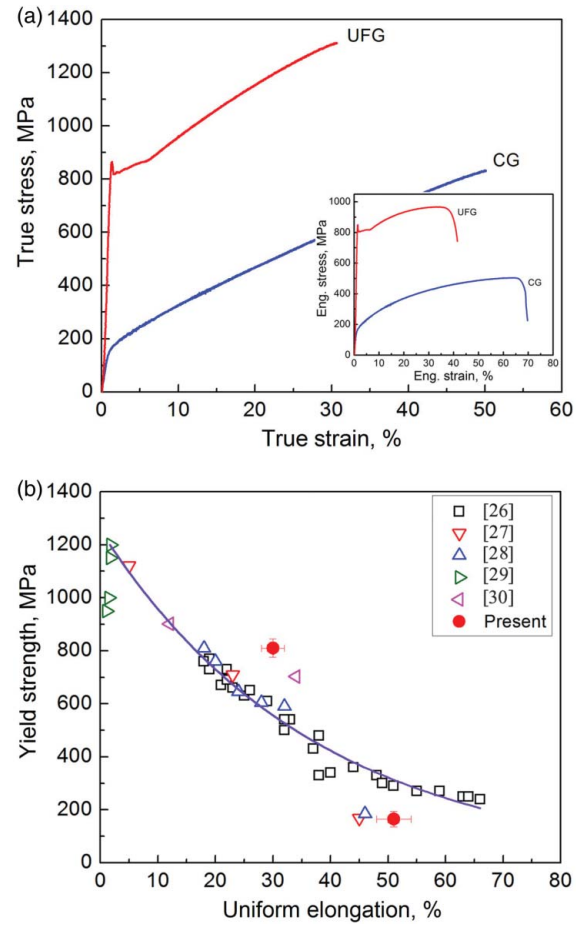

Figure 2. (a) Typical tensile true stress–strain curves for UFG and CG 304 L SSs at a quasi-static strain rate of $5 \times 10^{-4}\ s^{-1}$ and RT. The inset is engineering stress–strain curves, (b) excellent strength–ductility combination of the current ideal UFG SS in comparison with other 304 L SSs (with Ni content of 10 ~ 12%).

of straight lines lying on the $(1\bar{1}1)$ plane, with lengths of several tens to hundreds of nanometers and interline spacing of 4 ~ 60 nm. The selected-area diffraction (SAD) pattern shows obvious streaks along the $[1\bar{1}1]$ direction, indicating that these lines are edge-on SFs. The formation of high density of SFs is due to the low SFE of this 304 L SS, ~34 mJ/m^2.[37] Low SFE promotes the dissociation of a full dislocation into two partial dislocations during plastic deformation. In UFG and nanocrystalline materials, the leading Shockley partial dislocations can originate from GBs and glide into grain interiors, leaving behind wide SFs.[38–40] In low SFE materials, the SFs can be very wide, even across the entire grains, as shown in Figure 3(b).

Figure 3(c) and 3(d) show annealing nanotwins in two ultrafine grains. High densities of dislocations are clearly shown near some TBs, suggesting that TBs are effective in blocking and storing dislocations. It is also seen that the interaction between dislocations and TBs made TBs curved and deviate from the original straight

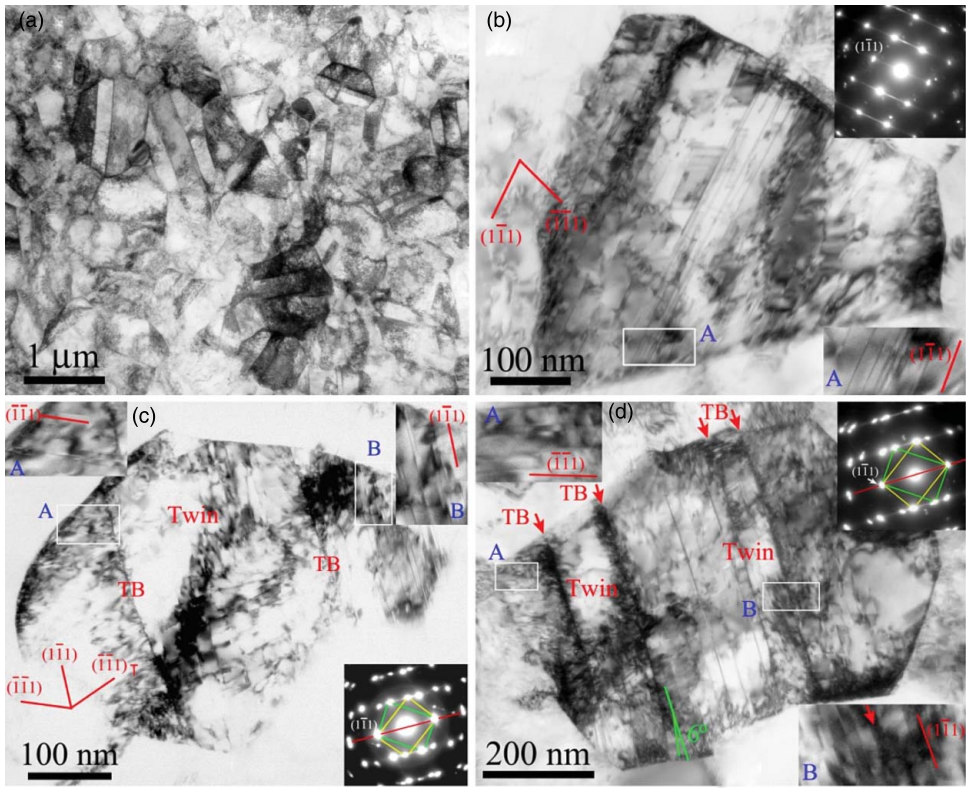

Figure 3. Typical TEM micrographs showing the microstructures and defects in ultrafine austenitic grains after ∼28% tensile strain: (a) overview of the microstructure, (b) defect structure in a 520 nm grain, (c) a 400 × 570 nm grain with an annealing twin, (d) a 500 × 700 nm grain with two nanotwins. The corresponding SAD patterns with [011] zone axis are shown in the insets. The insets denoted by capital letters A and B are enlarged from the corresponding white frame regions, which reveal different slip planes activated in different regions.

line, which is consistent with a previous report.[41] In addition, the nanotwins lead to activation of more slip systems for dislocations/SFs. As seen in the inset images enlarged from the corresponding white frame regions in Figure 3(c) and 3(d) (denoted by capital letters A and B), the dislocations/SFs on the left part of matrix glided on the $(\bar{1}\bar{1}1)$ plane, while on the right side they glided on the $(1\bar{1}1)$ plane. Within twin lamellae, the dislocations can glide on both $(1\bar{1}1)$ and $(\bar{1}\bar{1}1)_T$ slip planes, as evidenced by the rhombic grids in the center of Figure 3(c). It is expected that the activation of multiple slip systems produces high strain-hardening rate, because the simultaneous activation of different slip systems needs a higher shear stress,[42] and the dislocations from different slip systems may entangle and react with each other.[43] The dislocation density in deformed grains is measured to be about 1.8×10^{15} m^2.

The generation of SFs was also observed within nanotwin lamellae, as demonstrated by the straight lines indicated by arrows in Figure 4. These SFs either traveled across twin lamellae or terminated inside the twin. The lower-left inset is an HRTEM image viewed from the [011] zone axis, confirming that these lines are SFs. The SFs can originate from TBs via dislocation-TB reactions. As revealed by molecular dynamic simulation [44] and analytical model,[45] when a perfect 60° dislocation meets a TB, it can be dissociated into a 30° partial and a 90° partial. The partials can transmit across the TB to slip in the twin to produce SFs, depending on the orientation and magnitude of local stress. As shown in Figure 4, most of the SFs are originated from TBs, which is consistent with the above twin-dislocation interaction theory.

The above microstructure and defect observations indicate that the ideal UFG structure produced by phase-reversion annealing can effectively accumulate a high density of dislocations during uniaxial tensile test, which explains its high strain-hardening rate. The contribution of dislocation accumulation to the plastic flow stress can be evaluated by the Taylor dislocation hardening relation, $\sigma = M\alpha Gb\sqrt{\rho}$, where σ is the true flow stress, M is the Taylor factor, α is the material constant, G is the shear modulus, b is the Burgers vector, and ρ is the dislocation density accumulated in grain interior during plastic strain. In this study, the dislocation density after tensile test is as high as 1.8×10^{15} m^2, which can be considered accumulated during tensile deformation because the initial dislocation density is extremely low (see Figure 1(a)). Using the typical parameters for 304 L SS ($M = \sqrt{3}$, $\alpha = 0.28$,[46] $G = 78$ GPa and

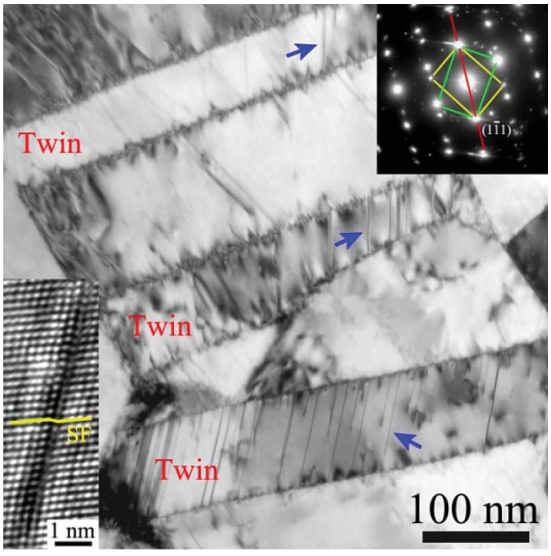

Figure 4. High density of SFs (indicated by arrows) formed inside nanotwin lamellae. The upper-right inset is corresponding SAD pattern with the [011] zone axis. The lower-left inset is an HRTEM image showing a stacking fault formed within a nanotwin.

$b = 0.2535$ nm), the increase in flow stress is calculated to be about 407 MPa. This value is close to the increase (470 MPa) of flow stress from yield point (810 MPa) to the true stress at 28% strain (1,280 MPa), as shown in Figure 2(a).

It should be noted that due to the low SFE of 304LSS, most dislocations are dissociated with SF ribbons, and some SFs have one or both ends pinned at GBs or TBs, as seen in Figures 3 and 4. This makes dislocation recovery via cross-slip and climb very difficult, because these processes require the wide SF ribbon to constrict into a full dislocation first. In addition, the SFs are effective barriers for blocking and accumulating dislocations.[47,48] When a moving dislocation encounters with a SF, it can either interact with the SF or accumulate near the SF if the applied stress is not high enough to activate the reaction.[45] It has been reported that SFs are very effective in promoting dislocation accumulation in UFG Cu–Zn alloy.[40] Therefore, lowering SFE has been found to enhance dislocation density and hence improve the strain-hardening rate of these alloys.[40,49–51]

Another important feature of the current UFG sample is the presence of a high density of nanotwins. These nanotwins must have contributed to the high strain-hardening rate. It has been reported that TBs are strong obstacles for blocking gliding dislocations and effective sites for storing dislocations,[44,45,51–53] which is also clearly shown in Figure 3(c) and 3(d). Lu et al. [54] proposed four types of TB-related dislocations to explain the strain hardening of nanotwinned Cu. They are glissile Shockley partials, sessile dislocation locks and extended SFs at TBs, as well as thread dislocations in the twin/matrix lamellae. All of these dislocations can be found in our samples, as shown in Figures 3 and 4. However, fabricating large bulk UFG materials with high density of nanotwins for structural applications is still a challenge to date. The current work provides a new approach to produce bulk low SFE UFG materials, which can be engineered with high density of annealing nanotwins for high strength and high ductility.

Other approaches have also been reported to improve the strength and ductility of UFG metals. For example, introducing nano-precipitates into the UFG matrix can recover some strain hardening. However, the increase in uniform elongation is still very limited, usually less than 10% in UFG Al alloys, for instance.[2,55] One approach for regaining high strain hardening is phase transformation, which can lead to high strength and good ductility in some austenitic steels.[18,30,56,57] For example, bulk UFG 301 grade austenitic SSs exhibited very high tensile yield strength (900–1,000 MPa) and high total elongation (30–40%) via strain-induced martensitic transformation.[18,19] However, the strain-induced martensite results in significant hydrogen embrittlement [31–33] and decreased corrosion resistance [34–36] in austenitic SSs, both of which are potential hazards for some applications such as nuclear reactor structural materials.[58,59] To avoid such problems, strain-induced martensite transformation has to be avoided during the plastic deformation of austenitic SSs. The ideal UFG structure produced by phase reversion in the current work avoids this problem and may have potential applications where resistance to hydrogen embrittlement and corrosion is critical.

In summary, we have produced an ideal UFG microstructure with fine grains, high density of annealing twins and low dislocation density by phase-reversion annealing of deformation-induced martensite in 304 L SS. It exhibited a superior combination of strength and ductility. The high strength resulted from the small grain size and high density of annealing twins, while the high ductility resulted from the high density of twins and initial low dislocation density, which were not only effective in blocking and storing dislocations, but also provided more room for dislocation accumulation. The low SFE of 304 L SS also helped with increasing the strain-hardening rate by producing SFs and dissociated dislocations with wide SF ribbons. These structural and deformation features ensured a high strain-hardening rate for high ductility. Finally, the ideal microstructure presented here can only be produced in fcc metals with low SFEs. Any other approaches that can produce fine grain size with high dislocation barriers and low dislocation density are expected to produce similar superior mechanical properties.

Acknowledgements This work was supported from National Natural Science Foundation of China (11172187 and 11172188). C.X. Huang acknowledges the Program for New Century Excellent Talents in University (NCET-12–0372) and Outstanding Young Scholars of Sichuan University (2012SCU04A05).

Supplementary online material. A more detailed information on experiments is available at http://dx.doi.org/10.1080/21663831.2014.968680.

References

[1] Zhu YT, Liao XZ. Nanostructured metals-retaining ductility. Nature Mater. 2004;3:351–352.
[2] Zhao YH, Liao XZ, Cheng S, Ma E, Zhu YT. Simultaneously increasing the ductility and strength of nanostructured alloys. Adv Mater. 2006;18:2280–2283.
[3] Zhao YH, Bingert JF, Liao XZ, Cui BZ, Han K, Sergueeva AV, Mukherjee AK, Valiev RZ, Langdon TG, Zhu YT. Simultaneously increasing the ductility and strength of ultrafine-grained pure copper. Adv Mater. 2006;18:2949–2953.
[4] Valiev RZ, Estrin Y, Horita Z, Langdon TG, Zechetbauer MJ, Zhu YT. Producing bulk ultrafine-grained materials by severe plastic deformation. JOM. 2006;58:33–39.
[5] Bay B, Hansen N, Hughes DA, Kuhlmann-Wilsdore D. Overview no. 96: evolution of fcc deformation structures in polyslip. Acta Metal Mater. 1992;40:205–219.
[6] Bay B, Hansen N, Kuhlmann-Wilsdore D. Deformation structures in light rolled pure aluminum. Mater Sci Eng A. 1989;113:385–397.
[7] Huang JY, Zhu YT, Jiang H, Lowe TC. Microstructures and dislocation configurations in nanostructured Cu processed by repetitive corrugation and straightening. Acta Mater. 2001;49:1497–1505.
[8] Meyers MA, Mishra A, Benson DJ. Mechanical properties of nanocrystalline materials. Prog Mater Sci. 2006;51:427–556.
[9] Witkin DB, Lavernia EJ. Synthesis and mechanical behavior of nanostructured materials via cryomilling. Prog Mater Sci. 2006;51:1–60.
[10] Valiev RZ, Langdon TG. Principles of equal-channel angular pressing as a processing tool for grain refinement. Prog Mater Sci. 2006;51:881–981.
[11] Saito Y, Tsuji N, Utsunomiya, Sakai T, Hong RG. Ultra-fine grained bulk aluminum produced by accumulative roll-bonding (ARB) process. Scripta Mater. 1998;39:1221–1227.
[12] Hausol T, Hoppel HW, Goken M. Tailoring materials properties of UFG aluminum alloys by accumulative roll bonded sandwich-lick sheets. J Mater Sci. 2010;45:4733–4738.
[13] Beyerlein IJ, Mara NA, Carpenter JS, Nizolek T, Mook WM, Wynn TA, McCabe RJ, Mayeur JR, Kang K, Zheng S, Wang J, Pollock TM. Interface-driven microstructure development and ultra high strength of bulk nanostructured Cu-Nb multilayers fabricated by severe plastic deformation. J Mater Sci. 2013;28:1799–1812.
[14] Zhilyaev AP, Langdon TG. Using high-pressure torsion for metal processing: fundamentals and applications. Prog Mater Sci. 2008;53:893–979.
[15] Park KT, Kim YS, Lee JG, Shin DH. Thermal stability and mechanical properties of ultrafine grained low carbon steel. Mater Sci Eng A. 2000;293:165–172.
[16] Yu YC, Kao PW, Chang CP. Transition of tensile deformation behaviors in ultrafine-grained aluminum. Acta Mater. 2005;53:4019–4028.
[17] Stolyarov VV, Zhu YT, Lowe TC, Valiev RZ. Microstructure and properties of pure Ti processed by ECAP and cold extrusion. Mater Sci Eng A. 2001;303:82–89.
[18] Somani MC, Juntunen P, Karjalainen LP, Misra RDK, Kyrolainen A. Enhanced mechanical properties through reversion in metastable austenitic stainless steels. Metall Mater Trans A. 2009;40:729–744.
[19] Misra RDK, Kumar BR, Somani M, KarJalainen P. Deformation processes during tensile straining of ultrafine/nanograined structures formed by reversion in metastable austenitic steels. Scripta Mater. 2008;59:79–82.
[20] Huang CX, Yang G, Deng B, Wu SD, Li SX, Zhang ZF. Formation mechanism of nanostructures in austenitic stainless steel during equal channel angular pressing. Phil Mag. 2007;87:4949–4971.
[21] Wu XL, Zhu YT. Inverse grain-size effect on twinning in nanocrystalline Ni. Phys Rev Lett. 2008;101:025503.
[22] Lu L, Shen YF, Chen XH, Qian LH, Lu K. Ultrahigh strength and high electrical conductivity in copper. Science. 2004;304:422–426.
[23] Lu K, Lu L, Suresh S. Strengthening materials by engineering coherent internal boundaries at the nanoscale. Science. 2009;324:349–352.
[24] Yoo CS, Park YM, Jung YS, Lee YK. Effect of grain size on transformation-induced plasticity in an ultrafine-grained metastable austenitic steel. Scripta Mater. 2008;59:71–74.
[25] Turtletaub S, Suiker ASJ. Grain size effects in multiphase steels assisted by transformation-induced plasticity. Inter J Solids Mech. 2006;43:7322–7336.
[26] Mataya MC, Brown EL, Riendeau MP. Effect of hot-working on structure and strength of type 304 L austenitic stainless steel. Metall Trans A. 1990;21:1969–1987.
[27] Qu S, Huang CX, Gao YL, Yang G, Wu SD, Zang QS, Zhang ZF. Tensile and compressive properties of AISI 304 L stainless steel subjected to equal channel angular pressing. Mater Sci Eng A. 2008;475:207–216.
[28] Huang CX, Yang G, Gao YL, Wu SD, Zhang ZF.: Influence of processing temperature on the microstructures and tensile properties of 304 L stainless steel by ECAP. Mater Sci Eng A. 2008;485:643–650.
[29] Ravi Kumar B, Mahato B, Sharma S, Sahu JK. Effect of cyclic thermal process on ultrafine grain formation in AISI 304 L austenitic stainless steel. Metall Mater Trans A. 2009;40:3226–3234.
[30] Ravi Kumar B, Raabe D. Tensile deformation characteristics of bulk ultrafine-grained austenitic stainless steel produced by thermal cycling. Scripta Mater. 2012;66:634–637.
[31] Eliezer D, Chakrapani DG, Altstetter CJ, Puch EN. The influence of austenite stability on the hydrogen embrittlement and stress-corrosion cracking of stainless steel. Metall Trans A. 1979;10:935–941.
[32] Han G, He J, Fukuyama S, Yokogawa K. Effect of strain-induced martensite on hydrogen environment embrittlement of sensitized austenitic stainless steels at low temperatures. Acta Mater. 1998;46:4559–4570.
[33] Zhang L, Wen M, Imade M, Fukuyama S, Yokogawa K. Effect of nickel equivalent on hydrogen gas embrittlement of austenitic stainless steels based on type 316 at low temperatures. Acta Mater. 2008;56:3414–3421.
[34] Hamada AS, Karjalainen LP, Somani MC. Electrochemical corrosion behavior of a novel submicron-grained

austenitic steel in an acidic NaCl solution. Mater Sci Eng A. 2006;431:211–217.
[35] Alvarez SM, Bautista A, Velasco F.: Influence of strain-induced martensite in the anodic dissolution of austenitic stainless steel in acid medium. Corros Sci. 2013;69: 130–138.
[36] Balusamy T, Sankara Narayanan TSN, Ravichandran K, Song park II, Lee MH. Influence of surface mechanical attrition treatment (SMAT) on the corrosion behavior of AISI 304 stainless steel. Corros Sci. 2013;74:332–344.
[37] Schramm RE, Reed RP. Stacking-fault energies of 7 commercial austenitic stainless-steels. Metall Trans A. 1975;6:1345–1351.
[38] Zhu YT, Liao XZ, Wu XL. Deformation twinning in nanocrystalline materials. Prog Mater Sci. 2012;57:1–62.
[39] Huang CX, Wang K, Wu SD, Zhang ZF, Li GY, Li SX. Deformation twinning in polycrystalline copper at room temperature and low strain rate. Acta Mater. 2006;54:655–665.
[40] Wang ZW, Wang YB, Liao XZ, Zhao YH, Lavernia EJ, Zhu YT, Horita Z, Langdon TG. Influence of stacking fault energy on deformation mechanism and dislocation storage capacity in ultrafine-grained materials. Scripta Mater. 2009;60:52–55.
[41] Cao Y, Wang YB, Chen ZB, Liao XZ, Kawasaki M, Ringer SP, Langdon TG, Zhu YT. De-twinning via secondary twinning in face-centered cubic alloys. Mater Sci Eng A. 2013;578:110–114.
[42] Seeger A, Diehl J, Mader S, Rebstock H. Work-hardening and work softening of face-centred cubic metal crystals. Phil Mag. 1957;2:323–350.
[43] Wu XL, Zhu YT, Wei GY, Wei Q. Strong strain hardening in nanocrystalline nickel. Phys Rev Lett. 2009;103:205504.
[44] Jin ZH, Gumbsch P, Albe K, Ma E, Lu K, Gleiter H, Hahn H. Interactions between non-screw lattice dislocations and coherent twin boundaries in face-centered cubic metals. Acta Mater. 2008;56:1126–1135.
[45] Zhu YT, Wu XL, Liao XZ, Narayan J, Kecskes LJ, Mathauhu SN. Dislocation-twin interactions in nanocrystalline fcc metals. Acta Mater. 2011;59:812–821.
[46] Kassner ME. Taylor hardening in five-power-law creep of metals and Class M alloys. Acta Mater. 2004;52:1–9.
[47] Jian WW, Cheng GM, Xu WZ, Koch CC, Wang QD, Zhu YT, Mathaudhu SN. Physics and modeling of strengthening of metals by parallel stacking faults. Appl Phys Lett. 2013;103:133108.
[48] Jian WW, Cheng GM, Xu WZ, Yuan H, Tsai MH, Wang QD, Koch CC, Zhu YT, Mathaudhu SN. Ultrastrong Mg alloy via nano-spaced stacking faults. Mater Res Lett. 2013;1:61–66.
[49] Zhao YH, Zhu YT, Liao XZ, Horita Z, Langdon TG. Tailoring stacking fault energy for high ductility and high strength in ultrafine grained Cu and its alloy. Appl Phys Lett. 2006;89:121906.
[50] Huang CX, Hu W, Yang G, Zhang ZF, Wu SD, Wang QY, Gottstein G. The effect of stacking fault energy on equilibrium grain size and tensile properties of nanostructured copper and copper-aluminum alloys processed by equal channel angular pressing. Mater Sci Eng A. 2012;556:638–647.
[51] Huang CX, Hu WP, Wang QY. Strain-rate sensitivity, activation volume and mobile dislocations exhaustion rate in nanocrystalline Cu-11.1at%Al alloy with low stacking fault energy. Mater Sci Eng A. 2014;611:274–279.
[52] Zhu T, Gao HJ. Plastic deformation mechanism in nanotwinned metals: an insight from molecular dynamics and mechanistic modeling. Scripta Mater. 2012;66:843–848.
[53] Li N, Wang J, Misra A, Zhang X, Huang JY, Hirth JP. Twinning dislocation multiplication at a coherent twin boundary. Acta Mater. 2011;59:5989–5996.
[54] Lu L, You ZS, Lu K. Work hardening of polycrystalline Cu with nanoscale twins. Scripta Mater. 2012;66:837–842.
[55] Horita Z, Ohashi K, Fujita T, Kaneko K, Langdon TG. Achieving high strength and high ductility in precipitation-hardened alloys. Adv Mater. 2005;17:1599–1602.
[56] Ma YQ, Jin JE, Lee YK. A repetitive thermomechanical process to produce nano-crystalline in a metastable austenitic steel. Scripta Mater. 2005;52:1311–1315.
[57] Huang CX, Yang G, Wang C, Zhang ZF, Wu SD. Mechanical behaviors of ultrafine-grained 301 austenitic stainless steel produced by equal-channel angular pressing. Metall Mater Trans A. 2011;42:2061–2071.
[58] Scott P. A review of irradiation assisted stress corrosion cracking. J Nucl Mater. 1994;211:101–122.
[59] Zinkle SJ, Was GS. Materials challenges in nuclear energy. Acta Mater. 2013;61:735–758.